

Stellar Coronagraph Using the Principle of Achromatic Null-Interferometer

A. V. Tavrov¹, O.I. Korablev¹, A. V. Rodin¹, I. I. Vinogradov¹, A. Yu. Trokhimovsky¹,
A. Yu. Ivanov¹, L. V. Ksanfomaliti¹, and D. A. Orlov²

¹ *Space Research Institute, Russian Academy of Sciences, Moscow, Russia*

² *Research Institute of High-Precision Instrument Engineering, Moscow, Russia*

Received May 14, 2009

Abstract—In order to observe exoplanets we propose a space-based achromatic stellar coronagraph combined with a 0.8–1.5 m telescope. We develop an achromatic common path interferometer for observing an exoplanet (a faint off-axis source) on the background of a host star (bright axial source). An image of the star and its copy acquire an achromatic phase shift by 180° and interfere in antiphase. The achromatic phase shift is caused by geometric phase in the scheme of a three-dimensional interferometer. The interference process divides spatially the dark and light fields of the star image redirecting them to the opposite sides of a beam splitter. The interference process does not weaken the image of a planet, with equal intensities it is redirected to both sides of a beam splitter. The suggested scheme of common path interferometer ensures mechanical stability. The background signal is experimentally demonstrated to be reduced by six orders of magnitude.

DOI: 10.1134/S0010952511020109

1. INTRODUCTION

In the nearest future leading world space agencies plan space missions for observation of exoplanets or extra-solar-system planets. For example, American space agency NASA plans two nearest space missions as a part of TPF (Terrestrial Planet Finder) project: multi-arm interferometer TPF-I (<http://planetquest.jpl.nasa.gov/TPF-I/TPFIwhitepaper.pdf> and http://planetquest.jpl.nasa.gov/TPF-I/tpf-I_index.cfm) with tentative date of launch in 2015–2020, and coronagraph TPF-C (http://planetquest.jpl.nasa.gov/TPF-C/tpf-C_index.cfm) in 2016. European space agency ESA actively promotes the project Darwin (http://www.esa.int/esaSC/120382_index_0_m.html) with a launch scheduled on 2018–2020. In Japan NASDA and JAXA agencies develop a program J-TPF (Japanese TPF) aimed at observations of exoplanets using the space telescope SPICA (<http://www.ir.isas.jaxa.jp/SPICA>) supplied with a coronagraph and scheduled to be launched in 2010. Powerful ground-based telescopes Keck (NASA) and Subaru (Japan) are supplied with coronagraphic modules (for example, HICIAO [1]) with the aim of observing exoplanets. Operation of the ground-based coronagraph, such as CIAO coronagraph, remained limited in principle by imperfect systems of adaptive optics, especially for the mode of exoplanet observation, where there is a lack of quality of active dynamic correction of the wave front, distorted by turbulence of the atmosphere, in order to

reach diffraction resolution of the telescope. The wave front quality for reaching a coronagraphic contrast of 10^6 is required $\lambda/600$ at the wavelength $\lambda = 1 \mu\text{m}$.

Star coronagraphy makes actual the problem of creating an achromatic astronomical instrument for visual optical and infra-red ranges [2, 3, 4]. Integral brightness of exoplanets in astronomical observations is less than the star brightness by 6–10 orders of magnitude, depending on wavelengths, from infra-red (IR) to visual range, respectively. In the Bracewell method [5] a long-base interferometer uses two telescopes in order to improve resolution; light from a background axial source (star) has a phase shift by π radians and destructively interferes. Simultaneously, light from an off-axis source (planet) interferes with another phase difference so that the off-axis source is attenuated insignificantly and has a signal level sufficient for photo recording. In recent time various optical devices are suggested for attenuation of the background star signal. Among them there are phase [6–7] and focal [8] masks, also used are apodization of the entrance pupil [9], delay lines [10], achromatic phase-shifting devices [11], and their combinations [12].

Null-interferometer removes background illumination by way of achromatic phase delay by π radians star coronagraphy [11].

Achromatic interference coronagraph [13] uses a scheme of Michelson interferometer with zero optical path difference (OPD). One arm of the interferometer

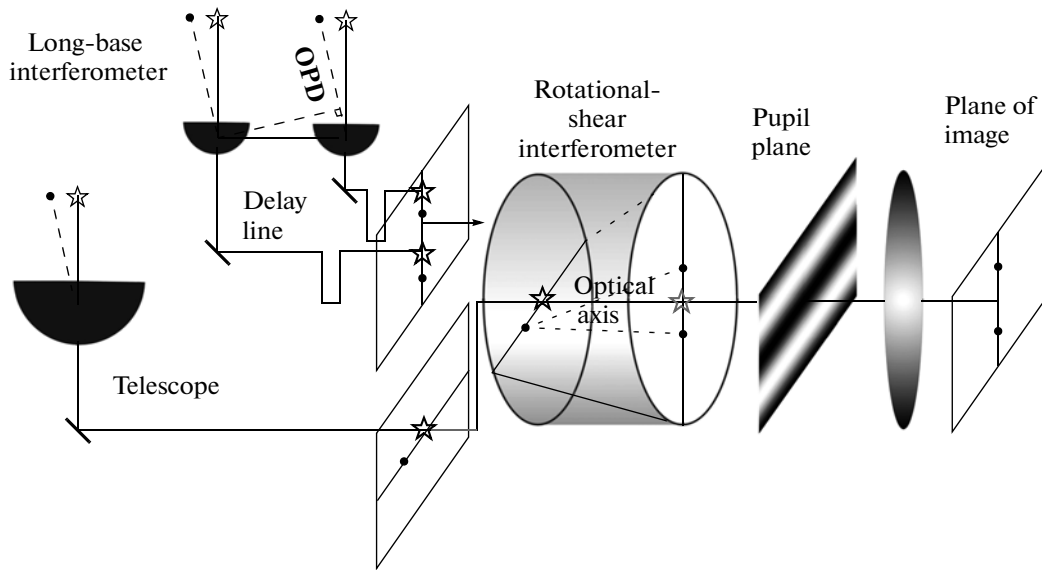


Fig. 1. Principle of attenuation of background axial signal.

includes spherical and parabolic mirrors for focusing and collimation, while another arm of the interferometer contains only plane mirrortrain. It is necessary to stabilize the interferometer OPD at approximately zero level with an accuracy of a few thousandth fractions of the wavelength ($\lambda/1000$), which is a technically difficult problem to be obtained in an interferometer with physically separated arms. Therefore, it is critically sensitive to small mechanical instabilities.

In recent publications [14–15] a new interferometer scheme was suggested that simultaneously introduces the achromatic phase shift by π radians (in order to reach dark field interferometer) and automatically eliminates undue sensitivity to mechanical instabilities owing to the common path scheme. Taking apart optical losses on the mirrors in the mode of linearly polarized light, the suggested interferometer divides the star light in the ratio 100%–0% and the planet light in the ratio 50%–50%, by redirecting corresponding energies to the different sides of a beam splitter, to *bright* and *dark* ports of the interferometer. The *bright* port of the interferometer receives 100% of starlight and 50% of planet light. The *dark* port of the interferometer receives only 50% of emission of the planet which is observable in the dark field of the star attenuated by a factor of 6–10 orders of magnitude.

In order to attenuate natural nonpolarized light, the starlight is divided in two orthogonal linear polarizations, and they are analyzed separately.

2. PRINCIPLE AND OPTICAL SCHEME OF THE RING ROTATIONAL SHEAR NULL-INTERFEROMETER

The optical path difference (OPD) between two arms of the interferometer, as applied to long-base interferometry and coronagraphy problems, and shown in Fig. 1, is equal to zero in the case of a star (axial source) marked by asterisk. The null-interferometer produces a phase difference equal to π radian, caused by the geometrical phase effect. The dark interference field is redirected to the *dark* output of the null-interferometer. The null-interferometer is realized according to the scheme of a rotational shearing interferometer (RSI) [16, 17]. RSI is differential interferometer with geometrical turn of reference wave front.

The planet represented by point in Fig. 1 attains non-zero OPD, and in the pupil plane it demonstrates an interference picture with localization of a dark interference fringe centered on the optical axis of the rotational shear interferometer. If the full light of the planet (off-axis source) is collected by integration of the periodic interference picture over the entire pupil of the optical system, then the interferometer does not attenuate substantially the signal of the off-axis source which can have a signal level sufficient for photo-recording.

The Sagnac interferometer [18] provides for a stable zero OPD due to the fact that two arms of this interferometer are geometrically superposed, and two waves propagate along one and the same path in opposite directions.

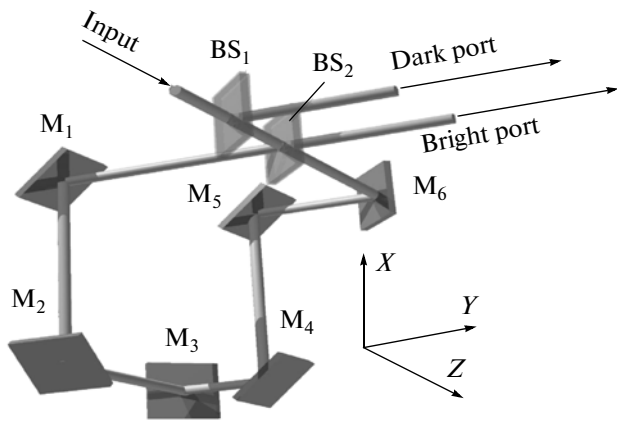


Fig. 2. Optical scheme of nonplanar null-interferometer.

In order to attenuate the background signal due to shifting geometrical phase, a three-dimensional (non-planar) scheme of the Sagnac interferometer is realized, radiation inside it propagating in three spatial coordinates (Fig. 2).

Non-planar scheme of the interferometer rotates polarization by azimuth angles of $+90^\circ$ and -90° , when waves propagate in the forward (clockwise) and backward (anti-clockwise) directions, respectively. The optical scheme of the interferometer includes six sequential flat mirrors designated as M_1-M_6 and two beam splitters BS_1 and BS_2 . The principal rays shown in Fig. 2 are directed along the interferometer arms. For example, the first arm of the interferometer is composed of the optical elements $BS_1-BS_2-M_1-M_2-M_3-M_4-M_5-M_6-BS_2-BS_1$. Another arm of the interferometer consists of the same optical elements installed in the opposite order: $BS_1-BS_2-M_6-M_5-M_4-M_3-M_2-M_1-BS_2-BS_1$.

Mirrors M_1-M_6 re-direct the principal ray along unit vectors of the three-dimensional space along three faces of the cube. Parallel (\mathbf{p}) and normal (\mathbf{s})

planes of reflection of the mirrors M_1-M_6 and beam splitter BS_2 cause rotations of polarization and image by $\pm 90^\circ$ when a light wave passes along the first and two interference arms [19].

Two waves having passed through the interferometer in the opposite directions attain a mutual geometrical turn of their images by 180° . The direction of oscillations of the light wave electric vector repeats the turn of an image, for example, in the case of dielectric mirrors with equal reflection coefficients \mathbf{p} and \mathbf{s} . The geometrical turn by 180° of the oscillation plane of the electric vector causes a phase shift of π radians as required for dark field interference. Destructive interference containing the dark field is localized from the side beam splitter BS_2 faced in the lateral direction to the entrance ray (Fig. 3).

Another output of the interferometer, light port, is located on the other side of beam splitter BS_2 faced oppositely to the course of incident ray. Beam splitter BS_2 separates the light and dark fields of interference, which is consistent with the energy conservation law: localization of the dark fringe on one side of the beam splitter corresponds to localization of the light fringe on another side of the beam splitter.

For an asymmetric beam splitter (for example, semitransparent plate) the electric vector turn forms a light field at reflection from the inner face of the beam splitter, and this takes place on the boundary faced from a material with larger optical density to a material with smaller optical density.

The electric field turn forms a dark field at reflection from the outer face of the beam splitter, on the material boundary from the smaller to larger densities. It is this fact that explains different orientations of the vector of electric field propagating over a common path along the interferometer arms [20].

For a completely symmetric beam splitter, for example, an ideal semitransparent cube, the phase shift by $\pi/2$ radians occurs upon reflection, and the

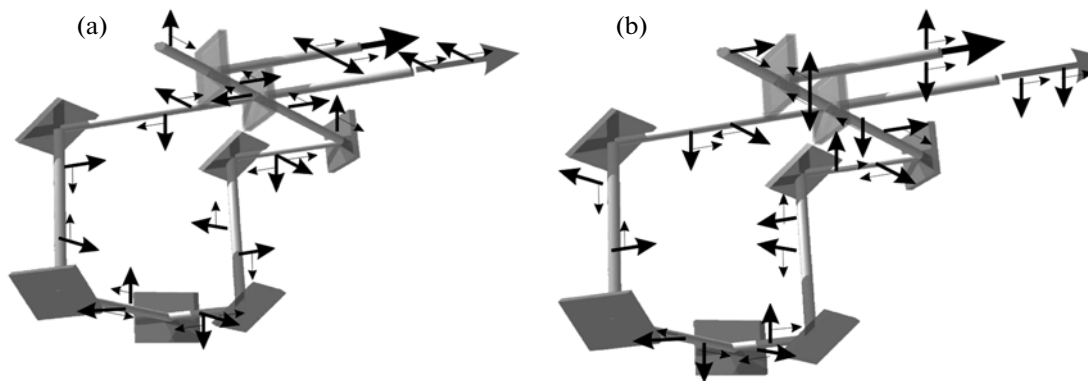


Fig. 3. Localizations of dark and bright fields on different sides of a beam splitter in two input polarizations: vertical (a) and horizontal (b).

fields at the interferometer output turn out to be shifted in phase by $2 \cdot \pi/2 = \pi$ radians.

The optical scheme of null-interferometer (Fig. 2) automatically compensates chromaticity of the beam splitters and mirrors due to propagation of two interfering waves along a single path in different directions. Two interfering waves have identical spectral intensities, which is a necessary and nontrivial condition for the dark field of destructive interference to make signal completely vanishing.

The beam splitter BS_1 serves for observing the *dark* output. BS_1 is designed as a broadband polarizing beam splitting cube for the visual range of wavelengths. The input radiation with vertical linear polarization passes through beam splitter BS_1 without substantial losses, and the interferometer analyzes the total energy of linearly polarized input radiation. The interferometer arms turn the azimuth of polarization of the input radiation by $\pm 90^\circ$, so that the output light attains polarization coinciding with the reflection mode of beam splitter BS_1 . The result of interference is again redirected without substantial losses to the *dark* output of the interferometer.

The image of a planet, directed to the interferometer and observed at the same dark output of the interferometer, shows another result: the plane wave propagates initially with a tilt relative to the interferometer axis on a beam splitter and is transformed by the interferometer in two waves also having a mutual tilt of their wave fronts. A focal of longitude interference fringes in the plane of the pupil of the optical system corresponds in the focal plane to two sources separated in space (Fig. 1). Thus, pair images of the planet (point-like off-axis sources) are geometrically separated in the image plane and, therefore, they do not interfere with each other.

Real diffraction images of the planet correspond to point spread function (PSF) of the optical system of telescope and interferometer that have a finite aperture. An off-axis source sufficiently close to the optical axis forms a small tilt of the wave vector to the interferometer axis, and two PSFs have a small lateral shift inside the main maximum (lobe) of PCF. A weakly resolvable source and its achromatic copy interfere in anti-phase, extinguishing each other only partially because of a lateral shift of PSF. For a scheme of generalized interferometric coronagraph this mode of null interferometer is considered in detail in [3], where a unique possibility of *super resolution* was demonstrated. The planet, inclined to the optical axis (pivoting axis of rotational shear interferometer) by an angle approximately twice lesser than the telescope angular resolution, has the maximum difference signal.

The null-interferometer of common path suggested in this paper is efficient for attenuation of radiation with linear polarization whose azimuth is ori-

ented at an angle of 45° to the interferometer branch. Limitations of the spectral range width for zeroed radiation are determined only by the transmission band of a material of the beam splitters. Chromatic characteristics of metal mirrors and coating of beam splitters are fully compensated. This compensation of chromatism is a unique characteristic of the suggested method. It allows one to perform measurements of off-axis source in the widest range of wavelengths technically possible at the present time.

Null-contrast depends on source size and takes on the following values for several practical sizes of a source: $NC\{0.006(\lambda/D)\} \approx 10^{-5}$, $NC\{0.002(\lambda/D)\} \approx 10^{-6}$.

These expressions correspond to theoretical limits of signal attenuation for stars with angular dimensions $1.2 \cdot 10^{-3}$ and $0.4 \cdot 10^{-3}$ arcsec, observed by a telescope with aperture of 1 m diameter at the wavelength $1 \mu\text{m}$.

Optical measurements under realistic conditions (extended source, finite precision of polarization installation, real mirror surfaces with residual micro-roughness and finite adjustment accuracy, etc.) are made with actual null-contrast lower than the theoretical value.

3. LABORATORY PROTOTYPE AND LABORATORY EXPERIMENTS

In order to demonstrate the effect of achromatic nulling of broadband emission of an axis source with the help of suggested null-interferometer and to measure its characteristics, we have designed a prototype of the interferometer. The optical block diagram of the experiment is presented in Fig. 4.

Two independent light sources were used: a halogen lamp of white light and a super-luminescent light diode (SLD). They were installed coaxially with interferometer axis and at a small inclination to it. Collimated beams of two light sources were combined by way of beam splitter BS_0 .

Measured spectral distributions of emissions of the halogen lamp and super-luminescent diode are presented in Fig. 5.

The halogen lamp emission (having passed through the glass bulb) has effective width of the Gaussian spectrum approximately 300 nm with a central maximum at about 570 nm. The band of emission of the super-luminescent diode is much narrower: effective width of the Gaussian spectrum is approximately 20 nm at a spectral maximum of 672 nm.

In order to improve spatial coherence the light of the above sources was transmitted through spatial filters. The narrowband emission of the super-luminescent diode was transmitted through a single-mode optical fiber after which almost completely spatially coherent light was obtained. The broadband emission of the halogen lamp by means of a condenser lens was

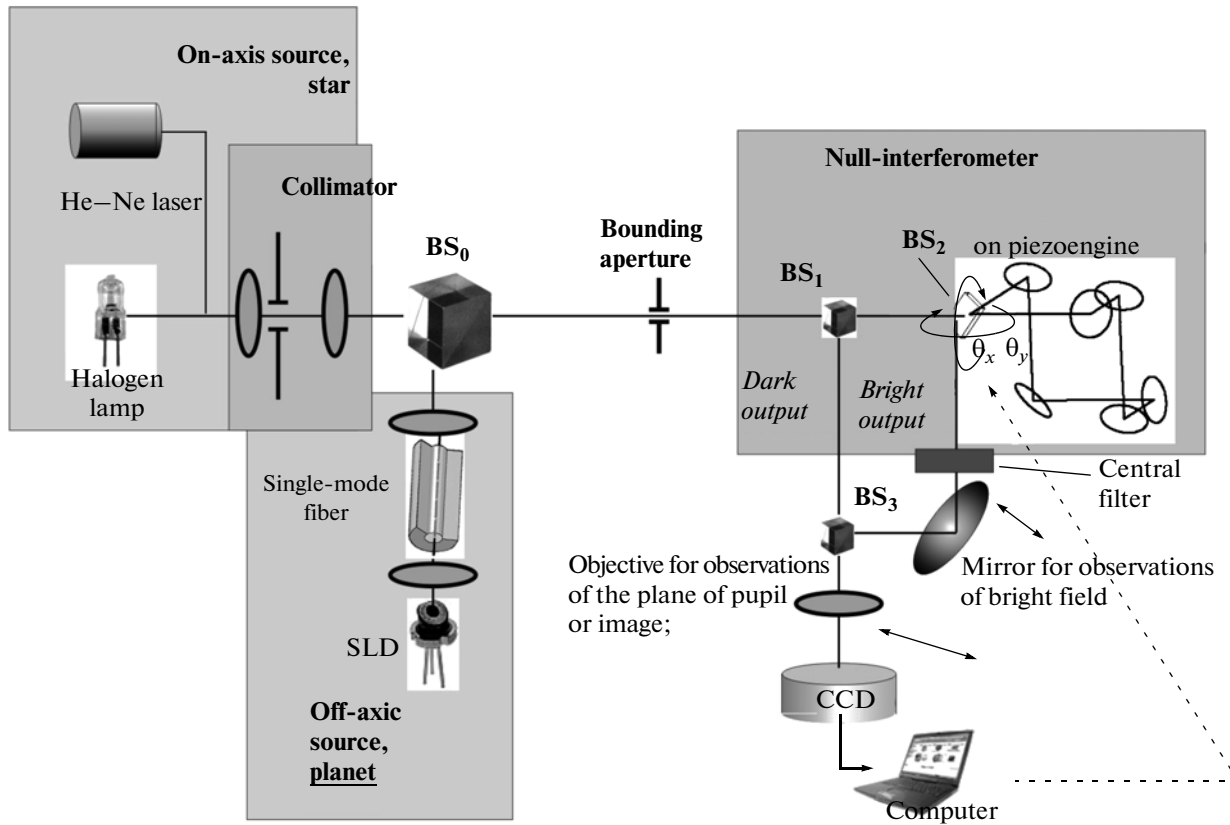


Fig. 4. Block diagram of the experiment.

collected on a stop that was placed at the focus of a collimator (achromatic lens).

For purposes of the experiment the axial sources of different angular sizes were needed, and they were created by changing parameters of collimation. For example, for visualization of the coherence region, in which interference fringes are observed with nonzero interference contrast, the effective angular size of the axial source was equal approximately to 12 minutes of arc. It was achieved by setting a stop diameter $20 \mu\text{m}$ and the focal length of the collimator 6 mm.

In order to reach then null-contrast of the axial source $NC \approx 10^{-3}$ in white light, the source's angular size equal to 10 arcsec was provided with a stop of $5 \mu\text{m}$ diameter and a collimator with focal length equal to 100 mm. The angular size of such a source expressed in Airy units of radius $[\approx \lambda/D]$ was equal to $\Theta \approx 0.02(\lambda/D)$ when observing in central wavelength $\lambda \approx 0.6 \mu\text{m}$ through a limiting stop $D = 0.2 \text{ mm}$.

Apparatus limitations for signal attenuation were studied with the spatially coherent light of a single-mode He-Ne laser.

The bounding aperture shown in Fig. 4 is optically conjugated with a pupil plane. By moving it in the lateral direction the optical axis of the interferometer was

preliminary centered with respect to the axis of a collimated source. For high-precision control of the interferometer axis inclination the beam splitter BS₂ was mounted on piezoengines providing for desired mechanical angles of tilt along axes Θ_x and Θ_y . Later on, the tilt was set by an external mirror installed in a holder with angular adjustment made by piezoceramic engines.

In the experiment a signal (attenuated due to destructive interference) from the *dark* output of the interferometer was compared to the *reference* signal received from the *bright* output of the interferometer. This *bright* output included the attenuator, a calibrated neutral filter. Two optical signals received from the dark and light ports for their simultaneous detection were overlapped (with a small lateral mismatch) in the field of a photo receiving device (CCD camera) with the help of a *mirror* and beam splitter BS₃ shown in Fig. 4. Before the CCD camera an objective was installed or an optical system for imaging the pupil. In the latter case the field Lyot stop installed in the plane optically conjugate to the pupil plane obscures approximately 10%–20% of the outer diameter in order to reduce diffraction edge effects. At the same

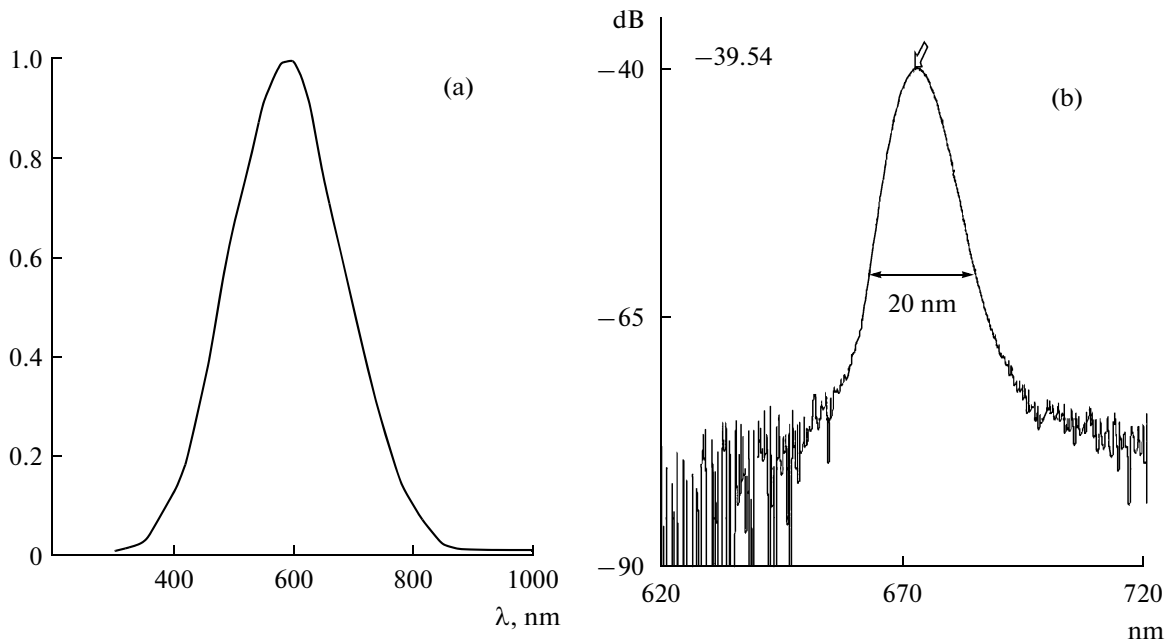


Fig. 5. Experimental spectral characteristics: of halogen white-light lamp (a) and super-luminescence diode (b).

time, the Lyot stop compensated lateral errors in alignment of the axes of the source and interferometer.

In more detail the functions of separate elements of the optical system are described when specifying particular experiments. The optical elements installed on movable holders for input into the optical scheme and output out of it are designed in Fig. 4 by symbol \leftrightarrow . Photos of the experimental setup in simplified and multifunctional modifications are shown in Fig. 6.

3.1. Visualization of the Coherence Area

The achromatic null-interferometer is installed in the pupil space of the optical system (Fig. 4). Originally, the CCD camera without objective was installed immediately at the *dark output* of the null-interferometer in order to observe a diffraction image of the pupil. The *bright output* of the null-interferometer was blocked, and the *mirror* shown in Fig. 4 was deflected. The axial (halogen lamp) and off-axis (super-luminescence diode) light sources were combined in the pupil plane by means of the beam splitter BS_0 . Figure 7 shows corresponding interference images which are easily identifiable immediately with each source. A ring-like central fringe of interference in Fig. 7a is produced by on-axis extended source. This is confirmed by the fact that only the halogen lamp was switched on electrically.

In Fig. 7b the rectilinear interference fringes with high frequency correspond to the off-axis light source having an inclination to the optical axis equal to

≈ 12 minutes of arc. Identification of the fringes is also easily checked by electrically switching on only the super-luminescence diode.

Figure 7c presents the interference pattern when both on-axis and off-axis sources are switched on simultaneously. Both the images show localization of dark interference fringes at the center corresponding to geometrical position of the null-interferometer axis. Figure 7c illustrates the principle of operation of an achromatic interference coronagraph that attenuates light of the axial source in order to detect on its weakened background the off-axis source light. Indeed, localizations of interference fringes are essentially different for the axial and off-axis sources. The emission of an off-axis source inherent in alternating interference fringes is detected on the background of a virtually dark field obtained as a result of destructive interference of the axial source emission. The residual (not completely attenuated) light of the axial source in Fig. 8c is caused by insufficient, small spatial coherence of the on-axis source (weak collimation). In the practical case of astronomical observation of a star, as an on-axis source, the radius of the central circular dark fringe of interference will be substantially increased due to increased spatial coherence of star light, and the background will become practically black because of destructive interference. In planned astronomy observations a solar-like star should have an angular dimension of a few milliseconds of arc, while the effective source dimension for a collimated halogen lamp in the prototypical experiment was equal to ≈ 12 minutes of arc.

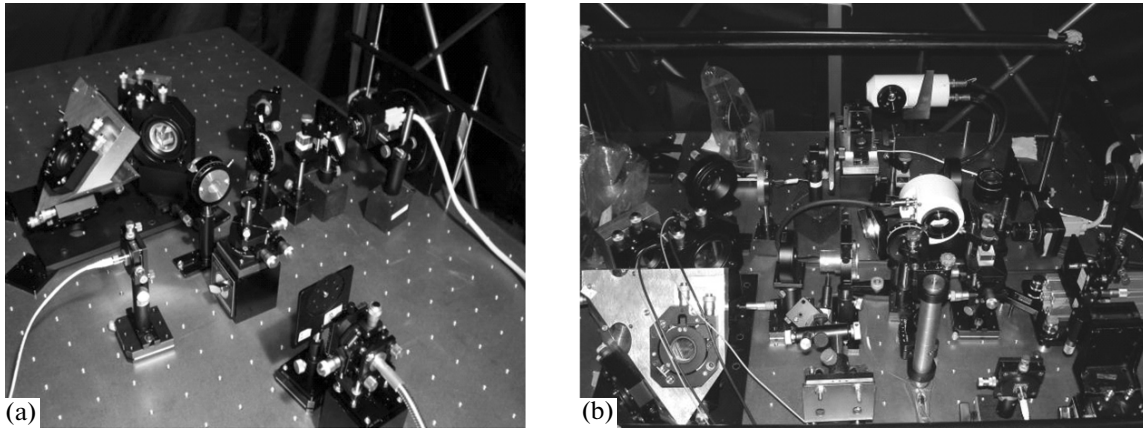


Fig. 6. Photographs of a simplified (a) and multi-functional (b) experimental setups.

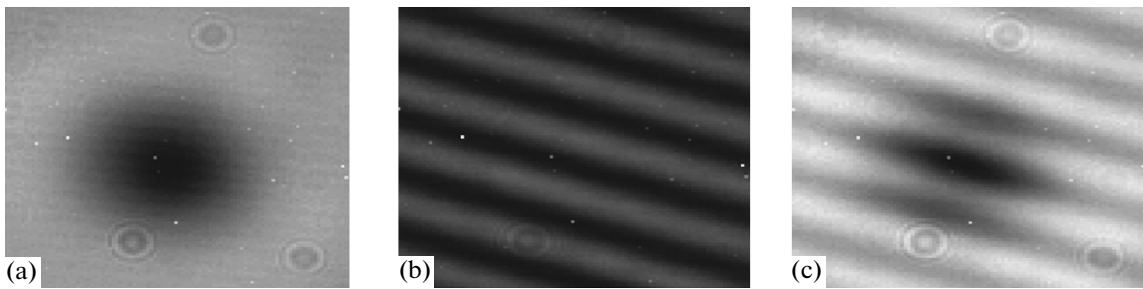


Fig. 7. Interference patterns observed in the pupil plane.

The behavior of interference contrast C (function of visibility of interference fringes) coincides with classical description [21] using first order Bessel functions of the first kind J_1 :

$$C = (I_{\max} - I_{\min}) / (I_{\max} + I_{\min}) = 2J_1(r') / r', \quad (1)$$

where $r' = 2\pi r\theta/\lambda$ is the optical coordinate, and θ is the angular size of a source.

The lateral dimension of the coherence region, its diameter $D_{\text{coherence}}$ corresponds to diffractometry theory [21] with a correction for diffraction propagation of an optical wave:

$$D_{\text{coherence}} \approx 3.83 \lambda_0 F / (d \pi) + 2 L \lambda_0 / D, \quad (2)$$

where F is the focal length of a collimator, d is the stop diameter determining the linear size of a source, λ_0 is the central wavelength, L is the distance from the collimator plane to the detector plane, and D is the collimator diameter.

The first term in formula (2) describes a lateral dimension of the coherence area in the collimator plane, while the second term corresponds to diffraction divergence of a beam in the space between the collimator and detector (CCD camera).

3.2. Achromatic Nulling in the Imaging Plane

In order to increase spatial coherence the effective size of the source was diminished down to angular size of approximately 10 arcsec, which corresponded to about $0.02 \lambda/D$.

Then, the observed diameter of coherence area reached approximately 16 mm and exceeded the linear dimension of a CCD camera chip equal to one third of an inch ≈ 8.47 mm. The boundary of the coherence area was not observed in the field of view of a lensless CCD camera in the pupil plane. For conversion into the imaging plane a standard objective was used to focus the pupil plane onto the CCD camera.

In order to demonstrate the effect of achromatic nulling in the interferometer the *dark* and *light* signals were divided on the beam splitter BS_2 (Fig. 4) and re-directed with the help of an additional beam splitter BS_3 into the field of view of the CCD camera for their simultaneous detection. When overlapping the dark and light signals in the field of view, a certain angular mismatch was set between the signals so that the *light* interference field was observed shifted upward from the *dark* field shifted downward. The elements *mirror* and *objective* of the optical scheme shown in Fig. 4 were included in the experiment scheme.

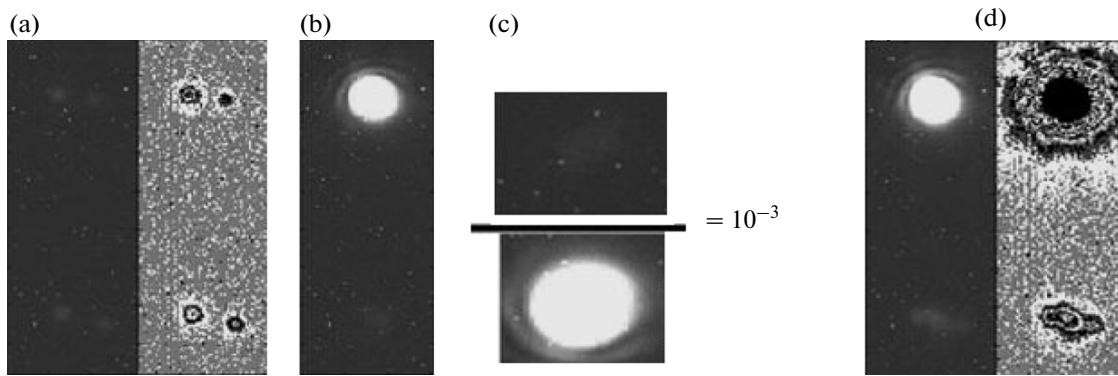


Fig. 8. Achromatic nulling.

According to energy conservation law, signals of the dark and bright outputs of the interferometer were observed to be complementary to each other: at destructive interference at the *dark* output the constructive interference was observed at the *bright* output. At alternating interference fringes corresponding to the off-axis source or at decreased coherence the signals become equal at two outputs of the interferometer. Therefore, the *bright* output intensity was used as a reference signal with which the attenuated signal was compared.

When observing the image of Fig. 8a only off-axis source was switched on electrically, and a pair of its images was observed at two outputs of the interferometer: *bright* output image is upper and *dark* is lower. Each element of the pair has intensity approximately equal to a quarter of the total power of the off-axis source and is located symmetrically about the optical axis of the interferometer. For visualization of null-contrast the off-axis source intensity was set three orders of magnitude lower than the intensity of the on-axis source.

In Fig. 8b only on-axis source of white light (collimated halogen lamp) was switched on electrically. The intensity of the on-axis source and the exposure time of the CCD camera were coordinated in order not to exceed the dynamical range of the CCD camera above its saturation. In the upper part of the field of view the on-axis source emission is observed in the *bright* output region. In the lower part a weak level of residual signal of non-zeroed axial source is detected.

For experimental measurement of nulling contrast NC in Fig. 8c the images of *bright* and *dark* fields, different in size, are compared. The digitized signal of photo counts at every point was summarized to calculate the integral intensity of fields. Their ratio amounts to a value of about three orders of magnitude, which is in agreement with estimation of a limiting theoretical nulling constrained by effective angular size $\approx 0.02 \lambda/D$ of an extended source.

In Fig. 8d the on-axis and off-axis sources of light are switched on simultaneously. In the upper region the *bright* field of the on-axis source completely surpasses in intensity the emission of a weak off-axis source. At the same time, in the lower region of the field of view the *dark* field of the axial source is sufficiently attenuated and adds only an insignificant background to the off-axis source. Light of the halogen lamp forming an off-axis source in this experiment had continuous spectrum with a width of about 300 nm, which indicates to full achromatism of nulling. The exposure time of the CCD camera was about 4 s, which testifies mechanical stability of the null-interferometer.

3.3. Nulling of Spatially Coherent Light of He–Ne Laser

The purpose of experiments on nulling the laser light source was to study limiting attenuation of light. Since the factor of insufficient spatial coherence was eliminated by way of using laser emission, other instrumental factors limiting the contrast of axial signal attenuation were studied.

3.3.1. Nulling in the Space of Pupil. As in the previous case, in order to compare intensities of the *bright* and *dark* outputs of the interferometer their signals were combined in the CCD camera plane with a small vertical shift. For simultaneous comparison of the intensities with a difference originally exceeding the dynamical range of the CCD camera ($\approx 10^3$) the emission of the *bright* output of the interferometer was attenuated by a calibrated neutral filter. For high-precision adjustment of the null-interferometer coaxially with the source axis piezoceramic engines were used to incline the beam splitter BS_1 (or, later, the external mirror not shown in Fig. 4).

Figure 9 shows the images on the pupil plane where the *dark* and *bright* outputs of the null-interferometer are presented in the lower and upper halves of the

CCD camera, respectively. The *dark* output of the interferometer include a contrast speckle-field, while the *bright* output demonstrates a more homogeneous distribution of intensity.

Emission from the *bright* output was attenuated by a neutral filter approximately by a factor of $2 \cdot 10^{-4}$.

The achromatic interference coronagraph (AIC) has the following property of image symmetry: if the incident ray at the input of the null-interferometer contains amplitude or phase image, then the *ideal* AIC summates two identical images rotated by 180° with respect to each other. At the output of the *ideal* AIC perfectly symmetrical images about the null-interferometer axis (symmetry axis) are observed. The real AIC consists of a system of sequential mirrors that provide for geometrical rotation of the image and electric vector. Local areas of an image are reflected actually from different parts of mirrors. If one takes into account residual micro-roughness of the mirrors, the ideal plane wave, due to reflection from a micro-relief (or scattering by it), produces an asymmetric image at the output, because of the fact that two waves propagating in opposite directions have no strictly common path. Micro-roughness creates a certain phase difference with spatial distribution (aberration). As a result, interfering wave packets will be summated with unequal aberrations due to their mutual rotations.

The asymmetric speckle-field is caused by residual micro-relief (micro-roughness) of mirrors. In order to reach a null-contrast of 10^{-6} , the micro-roughness should not exceed the maximum value $\lambda/3000$ PV (peak-to-value). In practice it is difficult to meet this requirement, taking into account that a wave front entering the interferometer is reflected from more than 16 optical surfaces, the number of planes being doubled at propagation of a ray in two opposite directions.

The maximum value of interference contrast obtained in experiment of Fig. 9 is about $2 \cdot 10^{-4}$. Then, the root-mean-square null-contrast averaged over the pupil plane has the value $NC_{rms} \approx 5 \cdot 10^{-5}$, which corresponds to root-mean-square value of the wave front surface $\delta_{rms} \approx \lambda/400$ at $\lambda = 630$ nm. The estimate $\lambda/400$ is equal to approximately a half of all aberrations of the wave front existing in the AIC system because of the fact that symmetrical components of aberrations are effectively eliminated by AIC, and they constitute approximately a half of all aberrations.

In Fig. 9 practically asymmetric speckle-field is observed, a more rigorous analysis of symmetric and asymmetric components of the speckle-field is presented in paper [22]. The observed speckle-field is caused by residual modulations of the wave front inside the null-interferometer.

The wave front distribution in the pupil plane is of fundamental importance for long-base interferome-

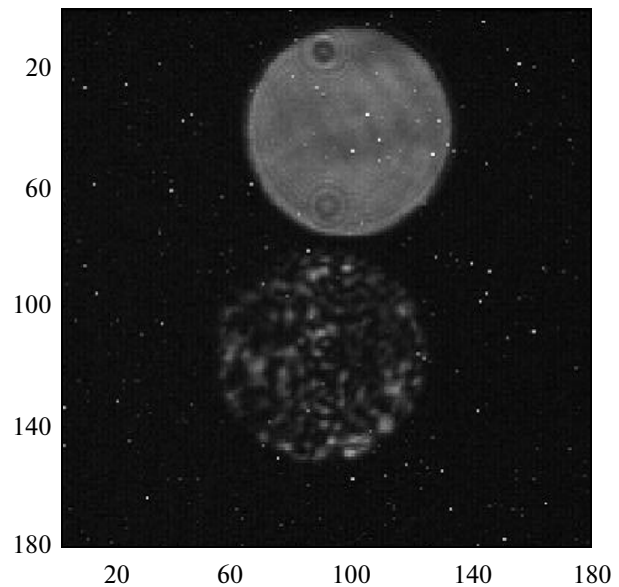


Fig. 9. *Dark* (top) and *bright* (bottom) field of interference.

ters. For the coronagraph, which records photoelectric signal in the image plane and is aimed at detection of an off-axis source in the local area of its image, the spatial distribution of the speckle-field as a function of distance from the axial source becomes essentially important. For investigation of the speckle-field distribution in the image plane over the pupil field, one needs to know not only intensity distribution, but phase distribution as well. In order to simplify the problem and to exclude high-precision measurement of the wave front in the pupil plane, direct measurement of the speckle-field intensity in the image plane is performed in the experiment, installing a focusing lens and relocating the CCD camera into the image plane.

3.3.2. Nulling in the Image Plane. At the wavelength $\lambda = 632.8$ nm the null-interferometer reached signal attenuation in the image plane down to peak value of $6.5 \cdot 10^{-6}$, as is shown in Fig. 10. To carry out these measurements, as in previous experiments, two outputs of the interferometer were simultaneously connected to the CCD camera with a certain linear shift: the *bright* output of the interferometer is shown up at bottom left, while the *dark* output is shown top right. The *bright* output signal was attenuated with a neutral filter by a factor of 10^5 .

During exposure in Fig. 10b the *bright* output of the interferometer was closed by a shutter so that the image fully repeated the *dark* output signal in Fig. 10b, represented by the residual speckle-field caused by instrumental errors of the null-interferometer.

Figure 11 presents linear cross-sections of intensity patterns for the *dark* output of the interferometer. The solid line corresponds to the cross-section in horizon-

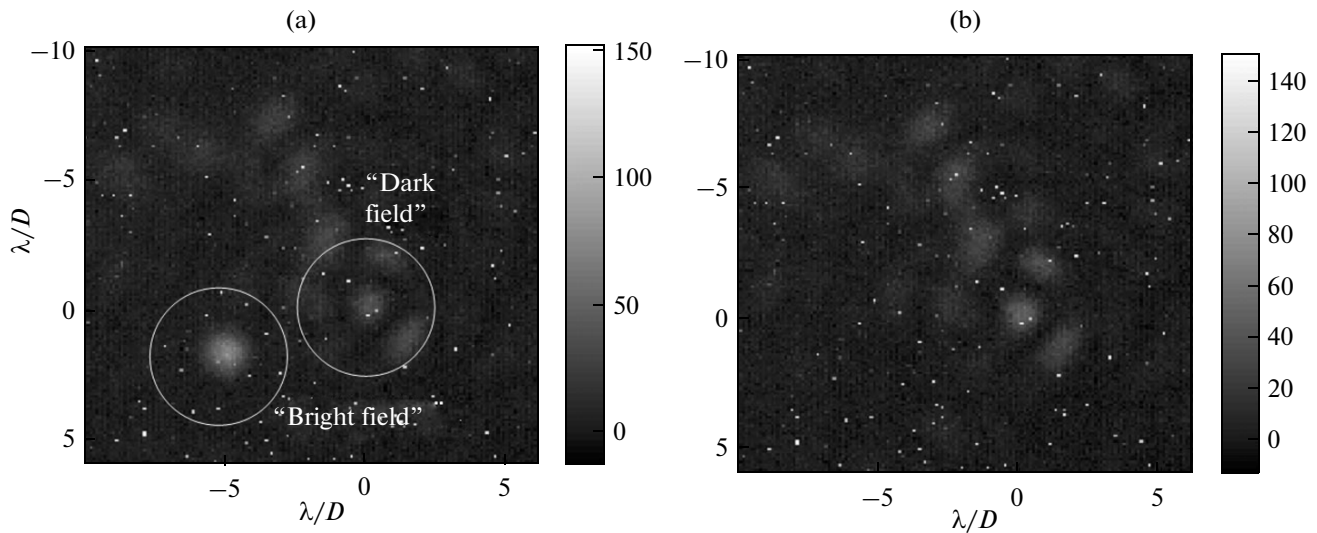


Fig. 10. Nulling in the image plane: (a) light and dark signals; and (b) only dark signal.

tal direction passed from the geometrical center – null-interferometer axis position – maximum signal of the *dark* output. The asterisk line corresponds to the cross-section obtained by averaging over all radial sections with origin at the center coinciding with the null-interferometer axis position. The averaged cross-section demonstrates attenuation of coherent signal below the level of 10^{-6} with angular position of a source $1 \cdot \lambda/D$, which is at the moment a record results obtained without correction of the wave front.

For these measurements the pupil of the optical system was conjugated with the plane where the Lyot stop was installed, next focusing to the image plane

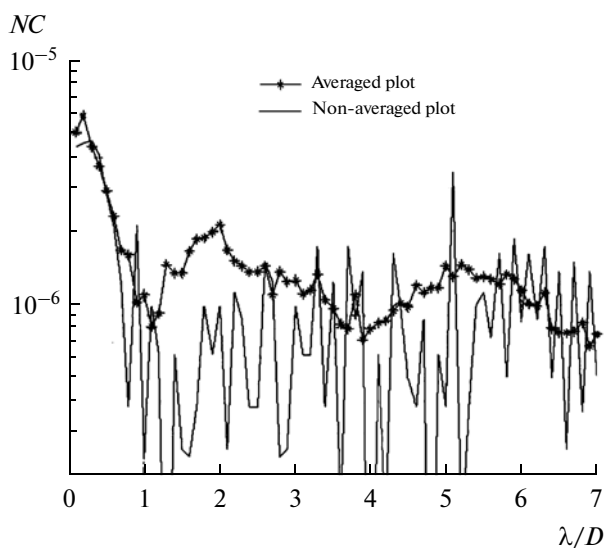


Fig. 11. Intensity profiles of the *dark* output of the interferometer.

was performed, where photorecording of the signal was made.

CONCLUSIONS

A new three-dimensional common path interferometer is suggested for an achromatic stellar coronagraphy: a high contrast suppressing an on-axis bright source (star) to observe an off-axis source (planet).

A laboratory experiment was carried out and demonstrated achromatic attenuation of axial signal with coronagraphic-contrast 10^{-3} over the visual spectral band 300 nm wide. By illumination with coherent laser light coronagraphic-contrast 10^{-6} has been demonstrated in the experiment for angular separation between the star and the planet $1 \cdot \lambda/D$. Other technical limitations were discussed, as well as practical feasibility how to improve the coronagraphic-contrast.

Presented null-interferometer in its implementation can be directly applied in the IR range, where the required coronagraphic-contrast is 10^{-6} .

ACKNOWLEDGMENTS

Fundamental principles of AIC were developed by a group of Nice Observatory headed by Y. Rabbia to whom the authors are grateful for overall support and constructive remarks. They also thank Japanese colleagues Y. Otani, Y. Takaki, T. Tanaka, T. Shieda, and T. Kurokawa from Tokyo University of Agriculture and Technologies, M. Pavlovsky and M. Takeda from Tokyo University of Telecommunications, and colleagues from National Astronomical Observatory J. Nishikawa, M. Tamura, and N. Murakami for their attention, discussions, and assistance. The work was partially supported by JSPS grant no. 18656018 and by

Programs Nanomaterials and SOE. B. Rinkevichus from Moscow Power Institute is thanked for comprehensive support and assistance in work. Partly the results of this paper were presented at Science and Engineering Conference “Optical methods of studying fluxes”, Moscow, 2009.

The work was partially supported by Federal Program “Scientific and Scientific-Pedagogical employes of innovative Russia (GK no. 02.740.11.0449). Another application of null-interferometer is possible for diagnostics of thermal fluxes.

REFERENCES

- Hodapp, K., Tamura, M., Suzuki, R., et al., HiCIAO: The Subaru Telescope’s New High-Contrast Coronagraphic Imager for Adaptive Optics: Adaptive Optics System, in *Ground-Based and Airborne Instrumentation for Astronomy II, Proceedings of the SPIE* McLean, I.S. and Casali, M.M., Eds., 2008, vol. 7014, p. 701419–12.
- Serabyn, E., Wallace, J.K., Hardy, G.J., et al., Deep Nulling of Visible Laser Light, *Appl. Opt.*, 1999, vol. 38, p. 7128.
- Baudoz, P., Rabbia, Y., and Gay, J., Achromatic Interfero-Coronagraphy, I. Theoretical Capabilities for Ground-Based Observations, *Astron. Astrophys. Suppl. Ser.*, 2000, vol. 141, pp. 319–329.
- Baba, N., Murakami, N., and Ishigaki, T., Nulling Interferometry by Use of Geometric Phase, *Opt. Lett.*, 2001, vol. 26, p. 1167.
- Bracewell, R.N., Detecting Nonsolar Planets by Spinning Infrared Interferometer, *Nature*, 1978, vol. 274, p. 780.
- Rouan, D., Riaud, P., Boccaletti, A., et al., The Four-Quadrant Phase Mask Coronagraph, *PASP—Publications of the Astronomical Society of the Pacific*, 2000, vol. 112, pp. 1479–1486.
- Roddier, F. and Roddier, C., Stellar Coronagraph with Phase Mask, *PASP—Publications of the Astronomical Society of the Pacific*, 1997, vol. 109, pp. 815–820.
- Tamura, M., Hodapp, K., Takami, H., et al., Concept of Science of HiCIAO: High Contrast Instrument for the Subaru Next Generation Adaptive Optics, in *Ground-Based and Airborne Instrumentation for Astronomy*, McLean, I.S. and Casali, M.M., Eds., 2006, vol. 6269, p. 62690V.
- Guyon, O., Pluzhnik, E., Galicher, R., and Martinache, F., Exoplanet Imaging with a Phase-Induced Amplitude Apodization Coronagraph. I. Principle, *Astrophys. J.*, 2005, vol. 622, pp. 744–758.
- van der Avoort, C., Mieremet, A., Pereira, S., and Braat, J., Demonstration of Nulling Using Delay Line Phase Shifters, in *New Frontiers in Stellar Interferometry, Proceedings of SPIE*, vol. 5491, Traub, W.A., Ed., Bellingham, WA: The International Society for Optical Engineering, 2004, p. 816.
- Rabbia, Y., Gay, J., Bascou, E., and Schneider, J.L., *Contract 14398/00/NL/MV Report (European Space Research and Technology Center, Noordwijk, Holland, 2001)*, rabbia@obs-azur.fr.
- Nishikawa, J., Kotani, T., Murakami, N., et al., Combination of Nulling Interferometer and Modified Pupil for Observations of Exoplanets, *Astronomy and Astrophysics*, 2005, vol. 435, pp. 379–384.
- Baudoz, P., Rabbia, Y., Gay, J., et al., Achromatic Interfero-Coronagraphy II, *Astron. Astrophys., Suppl. Ser.*, 2000, vol. 145, pp. 341–350.
- Tavrov, A., Tanaka, Y., Shioda, T., et al., Achromatic Coronagraph Based on Out-of-plane Common-Path Nulling Interferometer, in *New Frontiers in Stellar Interferometry, Proceedings of SPIE*, 2004, vol. 5491, Traub, W.A., Ed., Bellingham, WA: The International Society for Optical Engineering, 2004, p. 824.
- Tavrov, A., Kobayashi, Y., Tanaka, Y., et al., Common-Path Achromatic Interferometer-Coronagraph: Nulling of Polychromatic Light, *Opt. Lett.*, 2005, vol. 30, p. 2224.
- Serabyn, E., Wallace, J.K., Hardy, G.J., et al., Deep Nulling of Visible Laser Light, *Appl. Opt.*, 1999, vol. 38, p. 7128.
- Scholl, M.S. and Paez, G., Cancellation of Star Light Generated by a Nearby Star-Planet System upon Detection with a Rotationally-Shearing Interferometer, *Infrared Physics and Technology*, 1999, vol. 40, p. 357.
- Hariharan, P., *Interferometers. Handbook of Optics 2*, McGraw-Hill, New York: M. Bass, 1995.
- Tavrov, A., Miyamoto, Y., Kawabata, T., et al., Generalized Algorithm for the Unified Analysis and Simultaneous Evaluation of Geometrical Spin-Redirection Phase and Pancharatnam Phase in a Complex Interferometric System, *JOSA—Journal of Optical Society of America*, 2000, vol. A17, p. 154.
- Hecht, E., *Optics. Chapter 4.3.1*, 2 Edition, Amsterdam, 1995.
- Born, M. and Wolf, E., *Principles of Optics*, Oxford: Pergamon, 1970.
- Boccaletti, A., Riaud, P., and Rouan, D., Speckle Symmetry with High-Contrast Coronagraphs, *PASP—The Publications of the Astronomical Society of the Pacific*, 2002, vol. 114, pp. 132–136.

Copyright of Cosmic Research is the property of Springer Science & Business Media B.V. and its content may not be copied or emailed to multiple sites or posted to a listserv without the copyright holder's express written permission. However, users may print, download, or email articles for individual use.